Study of TES based microcalorimeters of different size and geometry under ac bias.

L. Gottardi*, H. Akamatsu*, J. van der Kuur*, S.J. Smith†, A. Kozorezov‡, and J. Chervenak †
*SRON Netherlands Institute for Space Research,
Utrecht, The Netherlands
Email: see http://www.sron.nl
†NASA Goddard Space Flight Center, Greenbelt, MD 20771, USA.
‡Department of Physics, Lancaster University, Lancaster, UK.

***Abstract*—Frequency-division multiplexing (FDM) is the current baseline read-out system for the large array of superconducting transition-edge sensors (TES's) under development for the X-ray instrument XIFU (*Athena*). In this multiplexing scheme the sensor operates as amplitude modulator of a MHz carrier. To achieve the best performance with these and similar instruments the detector physics and its interaction with the read-out circuit needs to be better understood. In particular we need an explanation for the dependence of the TES microcalorimeter non-linear impedance on the bias point, because it directly affects the choice of the detector optimal working point. With the TES microcalorimeters fabricated at NASA-Goddard we observe current steps in the amplitude of the uncalibrated IV characteristics when the detectors are read-out in the frequency domain and are biased in the low resistance part of the superconducting transition. In this paper we report on the characterization under FDM of NASA-Goddard TES microcalorimeters under development for the XIFU instrument. We have measured several pixels with different size and geometry in the bias frequency range from 1 to 4 MHz and at different bath temperatures. The results will be discussed within the recently developed weak-link theoretical framework.**

I. Introduction

At SRON, we are developing the Frequency-division multiplexing (FDM) read-out system of a large array of superconducting transition-edge sensors (TES's) for the XIFU [1] and the SAFARI [2] instruments on the future X-ray and infra-red space missions Athena and SPICA. A lot of progress has been made in the last years to understand the detector physics and a review has been recently published [3].

TES-based devices behave as weak-links due to longitudinally induced superconductivity from the niobium leads via the proximity effect [4], [5]. In our recent experimental works we have shown a clear evidence of the Josephson effects in ac biased TES bolometers and microcalorimeters [6], [7]. TES-based microcalorimeters are relatively more complex than bolometers. The microcalorimeters operate at larger bias current than bolometers, they are more sensitive to the self-generated magnetic field and the current flowing in the TES is not necessarily uniform due to the presence of normal metal structures employed to reduce the excess noise or to thermally couple the TES with the radiation absorber. TES current jumps, bistable effects and hysteretic behaviour have been recently reported in dc voltage biased TES microcalorimeters used in time-division multiplexers. With the TES microcalorimeters fabricated at NASA-Goddard we observe current steps in the uncalibrated amplitude of the $I-V$ characteristic when the detectors are read-out in the frequency domain [6], [8], [9] and are biased in the low resistance part of the superconducting transition.

The effects observed under ac bias could find a natural explanation within the resistively shunted junction (RSJ) model. In this paper we have studied the TES $I-V$ characteristic of several devices as a function of the bias frequency and bath temperature.

II. Detectors and read-out description

The devices under test are NASA-Goddard X-ray Mo/Au bilayer TES microcalorimeters from a uniform 8×8 array [10] and from a mixed array with different detector designs and configurations. In the uniform array the TES's are $150\,\mu\mathrm{m}\times 150\,\mu\mathrm{m}$ large and are coupled to a micron-thick overhanging $242\,\mu\mathrm{m}\times 242\,\mu\mathrm{m}$ Au/Bi X-ray absorber. The pixels have an intrinsic transition temperature of $T_{Ci}\sim 95\,\mathrm{mK}$, and a normal state resistance of $R_N = 8\,\mathrm{m}\Omega$. In the mixed array we have

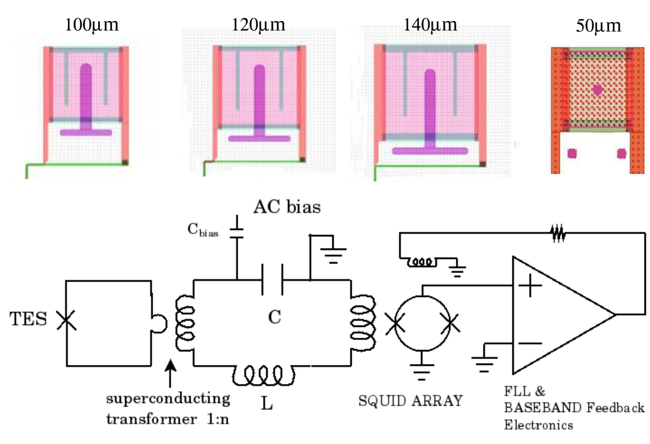

Fig. 1. *Top:* Layout of the pixels under test with $100\,\mu m\times 100\,\mu m$, $120\,\mu m\times 120\,\mu m$ and $140\,\mu m\times 140\,\mu m$ Mo/Au TES's deposited on a SiN membrane and a $50\,\mu m\times 50\,\mu m$ Mo/Au TES on Si substrate. All the TES are coupled to a $242\,\mu m\times 242\,\mu m$ Au/Bi absorber.*Bottom:* Schematic of the MHz read-out circuit. (Color figure online.)

tested four different pixel designs: a $50\,\mu\mathrm{m}\times 50\,\mu\mathrm{m}$ Mo/Au

TES on Si substrate with a central Au dot coupling to a $242\,\mu\mathrm{m} \times 242\,\mu\mathrm{m}$ Au/Bi absorber, and three pixel types with TES size respectively of $100\,\mu\mathrm{m} \times 100\,\mu\mathrm{m}$, $120\,\mu\mathrm{m} \times 120\,\mu\mathrm{m}$ and $140\,\mu\mathrm{m} \times 140\,\mu\mathrm{m}$, deposited on a SiN membrane and with a geometry similar to the uniform array pixels. The pixels in the mixed array have normal resistances of about 10 mΩ, a T_C between 95 and 100 mK, and a nominal thermal conductance G to the bath respectively of $700\,\mathrm{pW/K}$, $207\,\mathrm{pW/K}$, $250\,\mathrm{pW/K}$ and $310\,\mathrm{pW/K}$. The pixels layout is shown in Fig. (1).

For the ac measurements we use a FDM system similar to the one described in [8] and working in the frequency range from 1 to $4\,\mathrm{MHz}$. The readout, shown in Fig. (1), is based on a low noise two-stage SQUID amplifier fabricated at VTT [11], [12] and high-Q LC filters developed at SRON using superconducting Nb film and amorphous Si lithographic technology [13]. The LC filters used in this work have an inductance of $L = 2\,\mu\mathrm{H}$ and $L = 400\,\mathrm{nH}$ for the uniform and the mixed array respectively. Superconducting flux transformers with 8-to-1 and 5-to-1 ratio are used to optimize the impedance matching between the SQUID amplifier and the TES's. The SQUIDs, the LC-filters and the TES array chips are mounted on a copper bracket assembled on a removable probe of a cryogen-free dilution refrigerator from Leiden Cryogenics [14].

III. Experimental results

We measured the critical current I_c as a function of the bath temperature T_{bath} for several devices of the mixed array biased at different frequencies. A collection of all the I_c curves is presented in Fig. (2) as a function of T_{bath} normalized to the critical temperature T_c of the TES.

The critical current of similar devices measured under dc bias [15], [16] is also added to the data set. For the sake of clarity, when comparing critical currents, the peak current value of the ac current is used, since the transition to the normal state first occurs at the maximum current flowing into the TES. In the I-V characteristic under ac bias, the current and voltage are given in rms values. Close to T_c the critical current shows the typical exponential decay of a weakly linked superconductor and the values measured under ac and dc bias are consistent with each other. At low T_{bath} the critical currents measured under ac bias saturate at lower values, which depend on the bias frequency.

This is very likely caused by additional dissipation internally to the TES, which is sufficiently high to keep the device hotter than T_{bath}. As a matter of fact the contribution from the losses in the LC bias circuit and the superconducting transformers were measured, during a calibration run without the TES's, to be smaller than $5 \times 10^{-5}\Omega$.

An estimation of the magnitude of the ac losses is shown in Fig. (2)**b.**, where $r = P/I_c^2$ is plotted as a function of T_{bath}. P is the pixel power obtained from the calibration of the TES $I-V$ curves. The resistances derived from the $I_C(T_{bath})$ curve tend to a constant value at low temperature ranging from $1\,\mathrm{m}\Omega$ to $2.5\,\mathrm{m}\Omega$ depending on the bias frequency. The measured ac losses are a significant fraction of the TES resistances in particular at high bias frequencies. The losses are likely due to the presence of the normal metal structure on the TES calorimeters introduced to mitigate the detector noise. The losses measured in the superconducting state of the $50\,\mu\mathrm{m}$ TES pixel, which has only a small normal dot in the center of the TES for the thermal coupling to the absorber, are smaller than the pixels with normal bars, even at a high bias frequency. We need to further investigate whether the losses are generated for example by eddy currents or by more sophisticated proximity effects in the normal structures of the TES.

In Fig. (3) the TES in-phase current I_I and the quadrature current I_Q are shown as a function of the TES voltage for 5 pixels biased respectively at 1.3, 1.4, 1.8, 2.0 and $2.4\,\mathrm{MHz}$, at zero magnetic field ($B < 0.6\,\mu\mathrm{T}$) and $T_{bath} = 55\,\mathrm{mK}$. The TES current is calibrated by using the SQUID read-out circuit parameters and the voltage by using the power estimated in the normal branch of the $I-V$ curve given the TES normal resistance R_N. We assume the TES to be fully resistive at large bias voltage and we use the phase measured in the normal state to calibrate out any phase shift caused by the read-out circuit. A continuum phase shift during the TES transition, not fully understood and currently attributed to a non-ideal behaviour of the superconducting transformer, has been removed from the phase before calculating I_I and I_Q. A more detailed description of the calibration of TES $I-V$ characteristics under ac bias will be published in the near future.

For high TES voltage (i.e high TES resistance) I_I shows the typical $I-V$ characteristics of a voltage biased TES. At low bias voltage ($V < 0.1\,\mu\mathrm{V}$) (where the TES is supposed to become superconducting, but still shows a residual resistance) steps appear in the current with a complex, though reproducible, structure. This effect could be related to the excess losses inferred from the $I_C(T)$ curves presented above. More measurements with a larger variety of pixels are needed to gain more insight into this topic.

The quadrature current shows the oscillatory dependence on the bias voltage typical of the Josephson current and observed in the ac biased bolometers [7] as well. The Josephson current flowing in the TES is in general about $10 \div 20\%$ of the normal current. Being it $\pi/2$ out-of-phase with respect to the TES voltage, it is related to the reactive component of the TES impedance and it affects the dynamics of the detector. The more complicated structure observed at low bias voltage is related to the nature of the transition and the non-linear impedance of the TES. The effect is not fully understood yet and is still under investigation. It is worth noting that the exact shape of I_I and I_Q strongly depends on the shape of the TES transition, which is not necessarily identical for the pixels of the array under test.

We measured the $I-V$ curves as a function of bath temperature to understand how the oscillatory behaviour in the quadrature current depends on the total current flowing in the TES. The higher the bath temperature the smaller the current in the TES. The results are plotted in Fig. (4) for the pixel biased at $1.3\,\mathrm{MHz}$. The threshold at which the

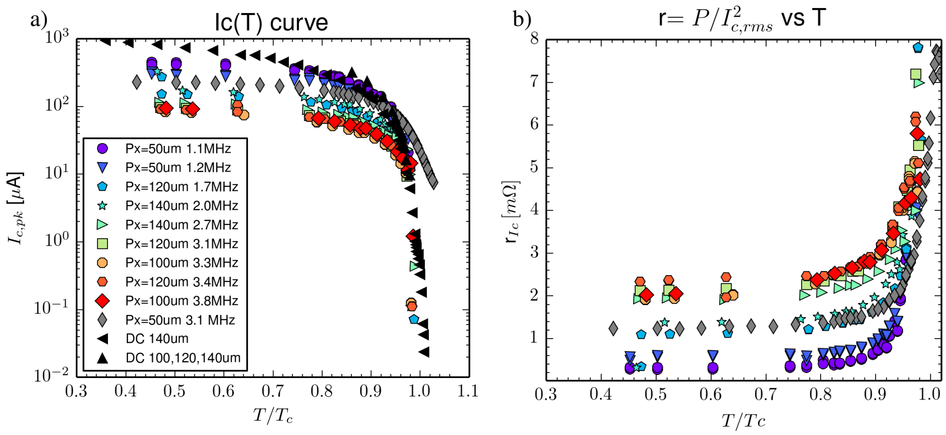

Fig. 2. **a.** $I_C(T)$ curves for several TES as a function of the normalized bath temperature T_{bath}. The black points are the critical current of similar devices under dc bias [15], [16]. **b.** Estimated losses $r = P/I_c^2$ from the critical current. (Colour figure online.)

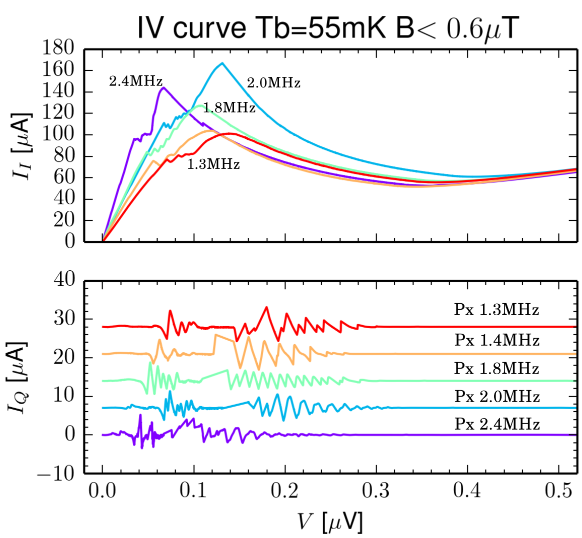

Fig. 3. I-V characteristics of the TES's as a function of bias frequency at $T_{bath} = 55\,\text{mK}$. Current in-phase *(upper plot)* and in quadrature *(lower plot)* with the voltage. The quadrature current for each pixel has been shifted vertically by $+7\,\mu$A for clarity. (Color figure online.)

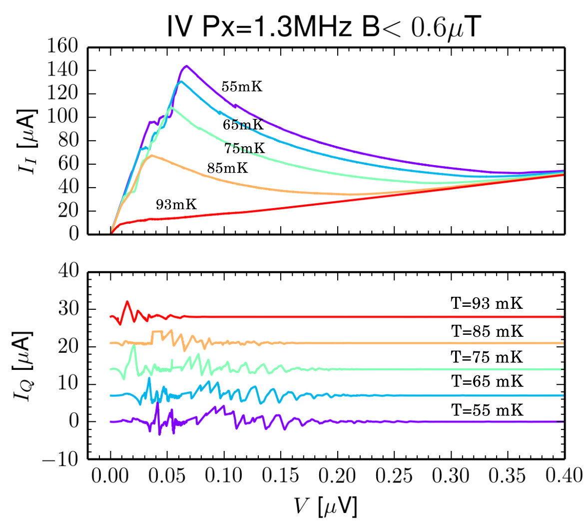

Fig. 4. I-V characteristics of a TES as a function of the T_{bath} for the pixel biased at $1.3\,\text{MHz}$. Current in-phase *(upper plot)* and in quadrature *(lower plot)* with the voltage. The quadrature current for each pixel has been shifted vertically by $+7\mu$A for clarity. (Color figure online.)

oscillations become visible in I_I moves to lower voltages at higher bath temperature, following the amplitude of I_I. This hints to the fact that the effect is mainly related to the detector impedance. The pixels from the mixed array show a behaviour similar to the $140\,\mu$m pixels from the uniform array reported above. From the I_I, I_Q and the calibrated TES voltage we can calculate the TES resistance and the reactance respectively.

Preliminary results are plotted in Fig. (5) for the 100, 120 and 140 μm devices of the mixed array, biased respectively at frequencies of 3.3, 1.7 and 2.7 MHz. The analysis of the $I-V$ curves of the $50\,\mu$m pixel has not been finalized yet and the results will be reported elsewhere. Here below we present a qualitative interpretation of the measurements for the larger pixels with normal metal bars.

The three devices show similar behaviour. It is important to note that the periodicity of the oscillation depends on the bias frequency as it follows from the standard weak-link theory and experimentally confirmed with TES bolometers [7]. Measurements done with similar pixels at different bias frequencies, not presented in this paper, do not show substantial difference from the data plotted here, except for the periodicity of the oscillations. The TES reactance is zero at large voltage when the pixel is in the normal state and it has an oscillatory dependence on the bias voltage at the superconducting transition. The reactance shows smooth oscillations at high resistance, which become sawtooth-like at low voltage bias.

We have calculated the TES non-linear impedance by solv-

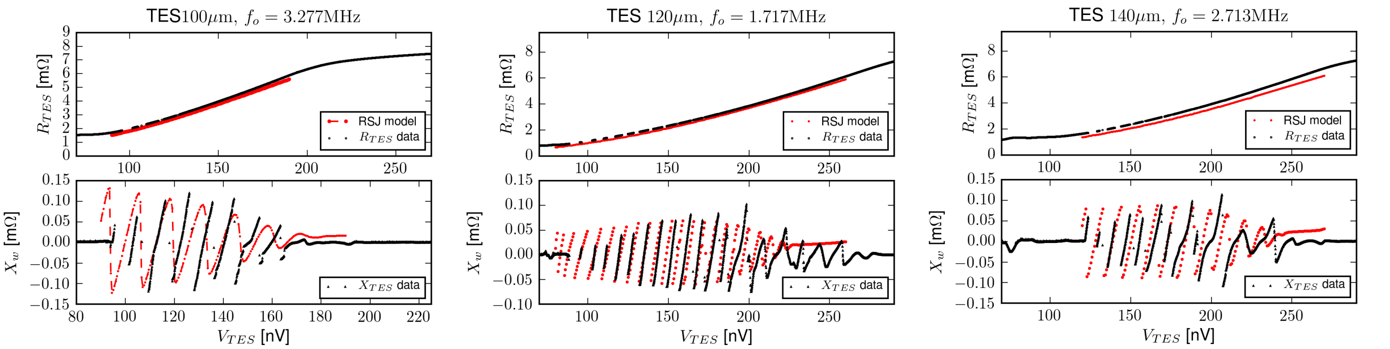

Fig. 5. TES resistance and reactance of the 100, 120 and 140 μm pixels. The red dashed curve shows the RSJ model applied to the TES's. (Color figure online.)

ing numerically the non-linear equation for the gauge-invariant phase across the weak-link under ac current biasing as derived from the RSJ model. We have followed the approach described in [17] in the limit of a small weak-link. The model considered here assumes uniform current distribution and neglects any possible contribution to the detector impedance from the normal structure and the self generated magnetic field inside the TES.

We used only the measured critical current and TES resistance as input parameters for the calculation. The results are plotted with red dashed curves in Fig. (5). This simple model fairly reproduces the major feature observed in the TES reactance. As explained in McDonald and Clem [17] the sharp changes in the reactance occur at values of the TES current for which there are bifurcations in the solutions of the non-linear equation. More details on the dependency of the solutions on the TES parameters will be presented in a future publication. To explain the fine structure observed in the experimental data a more sophisticated model is required. In particular we need to solve the resistive network to include the effect of the normal structure in the electrical resistance and make a realistic estimation of the current distribution in the device [18].

IV. Conclusion

We have studied the ac response of several TES microcalorimeters with different size and geometry. We discovered an additional internal dissipation mechanism in the ac biased TES calorimeter. The excess losses depends on the bias frequency and are particularly enhanced in TES with normal metal bars introduced to mitigate the detector noise under dc bias. For the large TES's with normal bars we have measured and analysed the $I-V$ characteristics. For all the devices, the quadrature TES current measured as a function of the TES voltage shows an oscillatory dependence, which is related to the nature of the resistive transition and to the behaviour of the TES as a weakly-linked superconductor. We have studied experimentally the dependency of the observed structures in the TES current as a function of the pixel geometry, the bias frequency and the bath temperature. The main features observed in the non-linear impedance of the TES microcalorimeters can be, at least qualitatively, explained using the RSJ model applied to a small uniform weak-link. A more sophisticated model that will include the effect of a non uniform current distribution in the TES is under development. From the preliminary results presented here, there is no evidence of a strong dependence of the detector response on the TES size. More tests have been planned for the future using a mixed array from NASA-Goddard with TES's with a larger variety of geometries.

Acknowledgment

We thank Kevin Ravensberg for his precious technical help. H.A acknowledges the support of NWO via a Veni grant. The research leading to these results has received funding from the European Unions Horizon 2020 Programme under the AHEAD project (grant a greement n. 654215). SRON is supported financially by NWO, the Netherlands Organization for Scientific Research.

References

[1] D. Barret et al., In Proc. SPIE Space Telescopes and Instrumentation 2016: Ultraviolet to Gamma Ray (2016).
[2] P. Roelfsema et al., In Proc. SPIE Space Telescopes and Instrumentation 2014: Optical, Infrared, and Millimeter (2014).
[3] J.N. Ullom and D.A. Bennett, *Supercond. Sci.Technol.* **28**, 084003, (2015) and D.A. Bennett *These Proceedings*.
[4] J.E. Sadleir, S.J. Smith,S.R. Bandler,J.A. Chervenak,and J.R. Clem, *Phys. Rev. Lett.* **104**, 047003, (2010).
[5] S.J. Smith, et al., *J. Appl. Phys.* **114**, 074513, (2013).
[6] L. Gottardi, et al. *J.Low Temp. Phys.* **167**, 214, (2012).
[7] L. Gottardi, et al. *Appl. Phys. Lett.* **105**, 162605, (2014).
[8] H. Akamatsu, et al. *J.Low Temp. Phys.* **176**, 591, (2014).
[9] H. Akamatsu, et al. *J.Low Temp. Phys.* **184**, 436, (2016).
[10] N. Iyomoto, et al., *Appl. Phys. Lett.* **92**, 13508, (2008)
[11] M. Kiviranta, et al., *J. Phys.: Conf. Ser.***507**, 042017, (2014).
[12] L. Gottardi, et al., *IEEE Trans. Appl. Superc.* (2015).
[13] M. Bruijn, et al.,*J.Low Temp. Phys.* **176**, 421, (2014).
[14] Leiden Cryogenics B.V., Leiden, The Netherlands.
[15] S.J. Smith, et al. *J.Low Temp. Phys.* **176**, 356, (2014)
[16] S.J. Smith, et al. *This Proceedings* (2016)
[17] J.McDonald and J.R.Clem *Physical Review B* **56**,14723, (1997)
[18] D.S. Swetz, et al. *Appl. Phys. Lett.* **101**, 242603, (2012)